A New Small Body Exploration Robot with Active Thermal Control

Takuma Honda*, Yosuke Miyata*, Tetsuo Yoshimitsu**, Takashi Kubota**

*Graduate School of Engineering, The University of Tokyo, Japan
**Institute of Space and Astronautical Science, Japan Aerospace Exploration Agency, Japan

Abstract

In recent years, small body exploration missions have been studied actively. Asteroids have some clues to know the origin of the solar system. In future missions, a wide range of surface exploration by small rovers is strongly expected. Asteroid exploration rovers are required to adapt to the asteroid environment because the gravity of asteroid surface is so low and very hot during the daytime. This paper proposes a new type of rover to move under microgravity as well as control its temperature by deploying the body of the rover. The effectiveness of the proposed rover is investigated by some simulations and microgravity experiments.

1 Introduction

In recent years, small body exploration missions have received a lot of attention. Asteroids may have better clues about the origin of the solar system because they were formed without thermal deformation[1]. A wide range of direct surface exploration by small rovers is important to investigate asteroid in detail. Asteroid exploration rovers are required to adapt to the asteroid environment. Required main functions are shown as below.

- **Robust mobility under microgravity environment** : The gravity of asteroid surfaces is very small, $10^{-7}\sim10^{-3}$[G]. In microgravity environment, it is difficult for rovers with wheeled mechanism to move. So, hopping mobility by pushing the surface is considered to be effective[2, 3, 4, 5, 6, 7] : In addition, moving mechanisms other than hopping are proposed[8, 9].
- **Countermeasures against heat environment** : Asteroid surface is very hot during the daytime and the daytime may be much longer due to the inclination of the rotation axis, rovers are required to have aggressive thermal control[10].
- **Simple mechanism** : Small and light mechanism is desirable because payloads are limited.

The conventional studies of the asteroid rovers focused only on mobility mechanism under microgravity. These rovers have not considered thermal control.

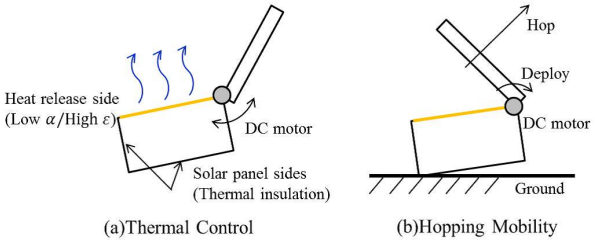

Figure 1. Concept of Deployment Rover

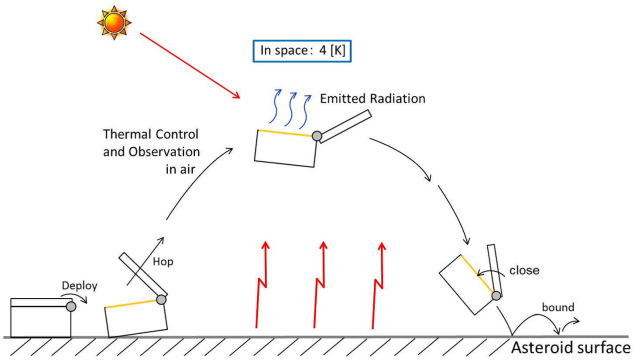

Figure 2. Scenario of Deployment Rover

In this paper, a new type of rover to move under microgravity as well as control its temperature by deploying the body of the rover is proposed. This paper shows the effectiveness of the proposed rover by some simulations and microgravity experiments.

2 Proposed Deployment-Type Rover

Figure 1 and Figure 2 show the concept of the proposed deployment rover and the exploration scenario respectively. The proposed rover has an actuator(DC motor) for deployment. So, the rover can hop and control its temperature. Figure 1(a) shows the deployment rover with a heat release side(low α/ high ϵ) on the inside and insulated outside. The rover can control its temperature actively by opening and closing heat release side hopping. Additionally, as shown in Figure 1(b), the rover can also hop by DC motor's torque and inertia force on the deployment part.

The deployment rover is to be considered very simple because hopping mobility and thermal control are realized by the same actuator.

Figure 2 shows the proposed deployment rover being insulated from external heat while staying on the surface. The rover hops to move to the destination. While hopping, the rover control its temperature by opening and closing the deployment part not to exceed the maximum allowable temperature. The rover is insulated again by closing just before landing. The deployment rover can move and control the inside temperature by repeating a sequence of these actions.

3 Active Thermal Control

In this section, the effectiveness of the thermal control of a deployment rover is investigated compared to a conventional passive model by using thermal mathematical model.

3.1 Thermal Design and Simulation Model

The thermal design models of a passive and a deployment rover are shown by Figure 3. The deployment rover has OSR(Optical Solar Reflector) as a heat release side on the inside. The sides other than the heat release side are not affected by heat from outside because the sides are insulated by MLI(Multilayed Insulation) and GFRP(Glass Fiber Reinforced Plastics). Additionally, rover body is externally covered with solar panels. This is to ensure that the rover obtains electricity regardless of the attitude. The rover can control the deployment part according to the external thermal environment and rover's temperature. Meanwhile, the passive model has no deployment part.

Coordinate system in thermal simulation is shown in Figure 4. The deployment rover consists of the deployment part(Body A) and main body(Body B). The face B_1 is the heat release side and the area is defined by L_E^2. The attitude angle of the rover is θ_R and the deployment angle is θ_{AB}. The passive rover is the model which does not have the deployment part(Body A). The rover also has heat source inside, from the on-board computer, Q_R.

Therefore, simulation settings are defined as follows : (i)No heat input from the insulation part. (ii)Asteroid surface is an infinite flat plane. (iii)The direction of the sun is constant. (iv)The rover moves only on the X-Z plane. (v)The rover always hops.

3.2 Thermal Control Method

The thermal control method of deployment rover is described here.

Thermal inputs to the asteroid rover are solar flux, albedo and infrared from the asteroid surface. There is some heat input to the rover even if the heat release side is directed towards the direction of the sun. This is because the heat release side has a low solar absorption. On the other, heat due to albedo and infrared from the asteroid surface are large in high temperature environment.

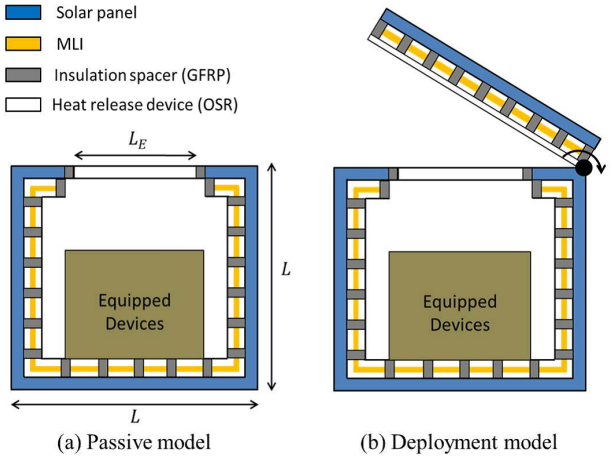

Figure 3. Thermal Design Model

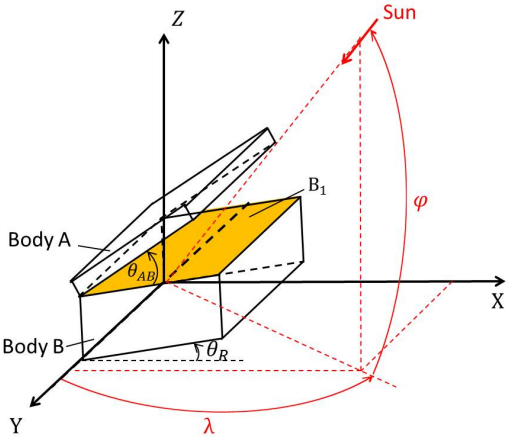

Figure 4. Coordinate System in Thermal Simulation

Therefore, the deployment rover closes the deployment part when the heat release side faces towards the surface. Meanwhile, the rover opens the deployment part when the heat release side directs to the space. The rover switches the deployment angle θ_{AB} as follows in accordance with the attitude angle θ_R.

- if $\theta_{Th1} < \theta_R < \theta_{Th2}$,

$$\theta_{AB} = 0[\text{deg}] \tag{1}$$

- elseif $\theta_{Th1} > \theta_R,\ \theta_R > \theta_{Th2}$,

$$\theta_{AB} = 180[\text{deg}] \tag{2}$$

Here, θ_{Th1} and θ_{Th2} are the thresholds of the attitude angle to switch the opening and closing of the deployment part. These thresholds can be calculate by comparing the allowable temperature and the equilibrium temperature of the rover for each attitude angle.

3.3 Simulation Study

Simulation parameters are shown in Table 1. The operating temperature range of the rover is defined as -30～60[degC].

The results of temperature analysis for the passive model are shown as Figure 5. These graphs show the temperature of the passive rover for time history in the case of the heat release area's variation(L_E^2=0.1^2～0.5^2[m^2]) and the internal heat's variation(Q_R=0～10[W]). These results show that the maximum rover temperature exceeds the allowable max temperature(60[degC]) even if the parameters of thermal design(L_E^2 or Q_R) are changed.

Next, the results of temperature analysis for the deployment model are shown in Figure 6. In the same way, Figure 6 shows the temperature for time history in the case of the heat release area's and the internal heat's variation respectively. The deployment rover can keep the temperature within the operation temperature if the parameters of thermal design are decided wisely. Thus, the deployment rover can operate in high temperature environment by active control.

4 Hopping mobility

In this section, the effectiveness of the proposed deployment rover in terms of hop mobility is investigated under microgravity. Additionally, a optimal design of the deployment rover is also shown.

4.1 2D dynamics model

A detailed 2D dynamic model of the deployment rover was deployed in our previous research[11]. The dynamic model is shown briefly.

2D model of the proposed deployment rover is shown by Figure 7. The deployment rover consists of Body A(the deployment part) and Body B(the main body) restrained at Point P_1. The rover is closed in the initial state and deployed to hop. Torque by DC motor acts around

Table 1. Parameters for Thermal Simulation

parameters	value
Intensity of solar radiation	1515 [W/m^2]
Albedo coefficient	0.1
Infrared emissivity	0.9
Absorptivity of OSR	0.1
Emissivity of OSR	0.8
Sun direction	λ=60[deg], ψ=85[deg]
Temperature of asteroid	140[degC]
Heat capacity of rover	1000[W·s/K]
Initial temperature of rover	30[degC]
Angular rate of rover	30[deg/s]

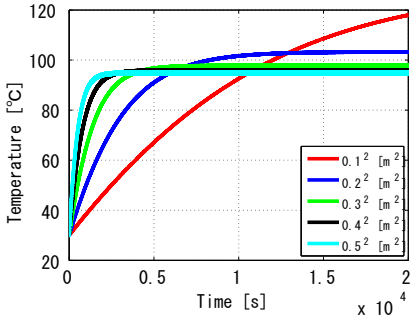

(a) Heat Release Area's Variation(Q_R=4[W])

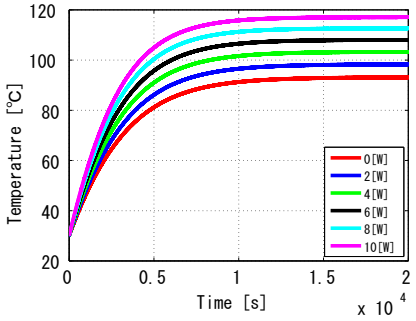

(b) Internal Heat's Variation(L_E^2=0.2^2[m^2])

Figure 5. Temperature for Time History of Passive Rover

the rover's body. Then, the body is inclined and lifted from the asteroid surface. The Equation of motion is constructed by multibody dynamics.

In hopping motion, the contact mechanics between the rover and the ground is important. Reaction force from the ground is derived by using penalty method. So, the reaction force is a spring-damper force which depends on the virtual settlement to the ground(Figure 8). The horizontal and vertical component of the reaction force is given by Equation (3)～Equation (5). F_{gx} and F_{gz} are the X and Z component of the reaction force. R_{gx}, R_{gz}, V_{gx}, V_{gz} are that of the settlement and the settlement's velocity. k_g and c_g are a spring and damper coefficient of the ground. Each μ and μ' are coefficients of static and dynamic friction of the ground.

$$F_{gz} = -(k_g R_{gz} + c_g V_{gz}) \quad (3)$$

$$F_{gx} = -(k_g R_{gx} + c_g V_{gx}) \quad (not\ slide) \quad (4)$$

$$= -sgn(V_{gx})\cdot\mu' F_{gz} \quad (slide) \quad (5)$$

The restraint condition is that the point P_1 is a rotation joint with torque. So, differential algebra type equation of motion for this dynamics model is shown in Equation (6). Here, $\mathbf{\Lambda}$ is Lagrange multiplier and γ is Baumgarte stabilization formula.

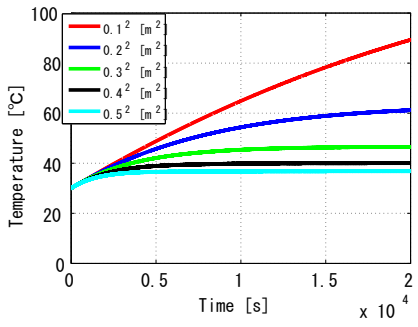

(a) Heat Release Area's Variation(Q_R=4[W])

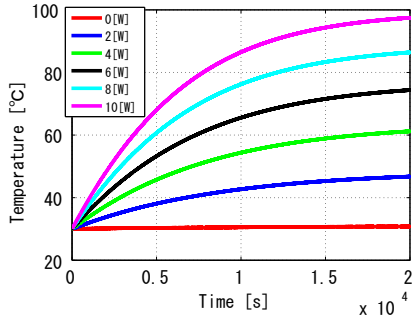

(b) Internal Heat's Variation(L_E^2=0.2^2[m^2])

Figure 6. Temperature for Time History of Deployment Rover

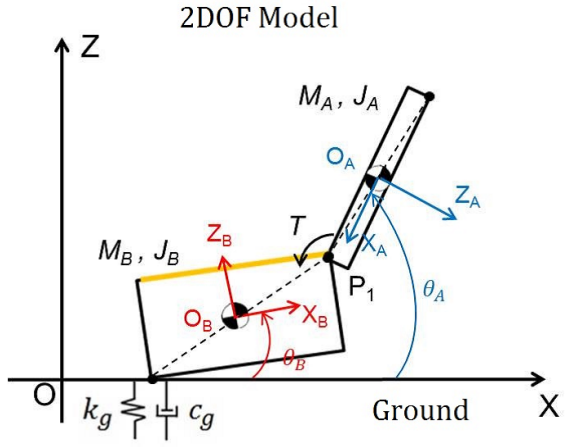

Figure 7. 2D Dynamics Model of Deployment Rover

$$\begin{bmatrix} \boldsymbol{M}_A & 0 & 0 & 0 & \boldsymbol{\Phi}^T{}_{V_{OA}} \\ 0 & J_A & 0 & 0 & \boldsymbol{\Phi}^T{}_{\omega_A} \\ 0 & 0 & \boldsymbol{M}_B & 0 & \boldsymbol{\Phi}^T{}_{V_{OB}} \\ 0 & 0 & 0 & J_B & \boldsymbol{\Phi}^T{}_{\omega_B} \\ \boldsymbol{\Phi}_{V_{OA}} & \boldsymbol{\Phi}_{\omega_A} & \boldsymbol{\Phi}_{V_{OB}} & \boldsymbol{\Phi}_{\omega_B} & 0 \end{bmatrix} \begin{bmatrix} \dot{\boldsymbol{V}}_{OA} \\ \dot{\omega}_{OA} \\ \dot{\boldsymbol{V}}_{OB} \\ \dot{\omega}_{OB} \\ \boldsymbol{\Lambda} \end{bmatrix} = \begin{bmatrix} \boldsymbol{F}_{OA} \\ N_{OA} \\ \boldsymbol{F}_{OB} \\ N_{OB} \\ \gamma \end{bmatrix} \quad (6)$$

,where

M_A, M_B	:	Mass of body A, B
J_A, J_B	:	Inertia moment of body A, B
$\boldsymbol{V}_{OA}$, $\boldsymbol{V}_{OB}$	:	Velocity of body A, B
ω_A, ω_B	:	Angular rate of body A, B
$\boldsymbol{F}_{OA}$, $\boldsymbol{F}_{OB}$	:	Acting force of body A, B
N_{OA}, N_{OB}	:	Torque of body A, B
$\boldsymbol{\Phi}$	:	Velocity constraint of each element

4.2 Simulation Conditions

The shape of the closed deployment rover is a square when viewed from above. The density of the rover is set to be a constant. Simulation parameter is shown in Table 2. Gravity acts vertically downward and the ground surface is given by a rock. $ratio_h$ denotes the ratio of the height of the deployment part for the overall height. An applied torque $T(t)$ is givens as follows. A constant torque is acted until the rover get off the ground. Then, after the rover has hop, a torque is applied to control the deployment angle to 180[deg].

Table 2. Rover Parameters for Hopping Simulation

symbol	meaning	value
M	Total weight	1.2[kg]
r	Width	120[mm]
h	Total Height	120[mm]
$ratio_h$	Deployment ratio	0.2
k_g	Ground's spring constant	10[kN/m]
c_g	Ground's damper constant	100[Ns/m]
μ	Static friction coefficient	0.5
μ'	Dynamic friction coefficient	0.4
g	Gravity	10^{-4}[G]
T	Constant torque	10^{-3}[Nm]

4.3 Assessment of Hop Mobility

The velocity of the deployment rover's center of gravity for time history is shown in Figure 9. This graph shows the deployment rover can obtain horizontal and vertical

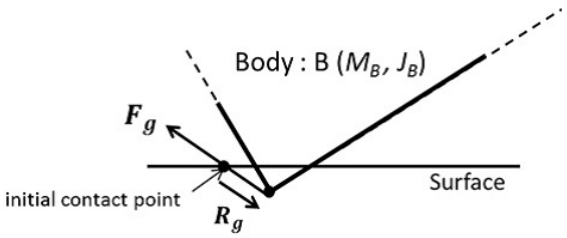

Figure 8. Contact Dynamics between Rover and the Ground

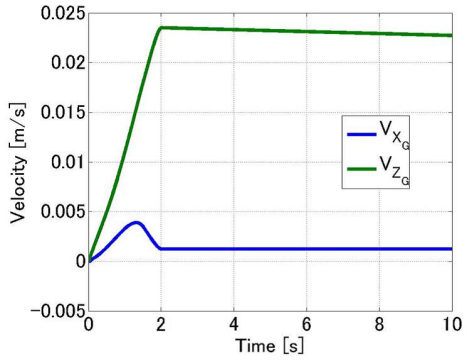

Figure 9. Velocity of Deployment Rover

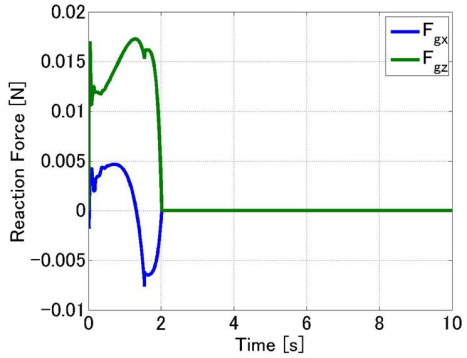

Figure 10. Reaction Force from The Ground

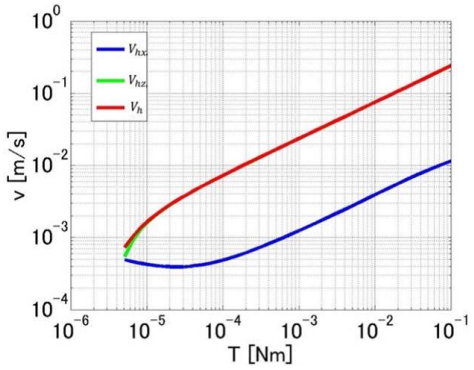

Figure 11. Hop Velocity for Torque's Variation

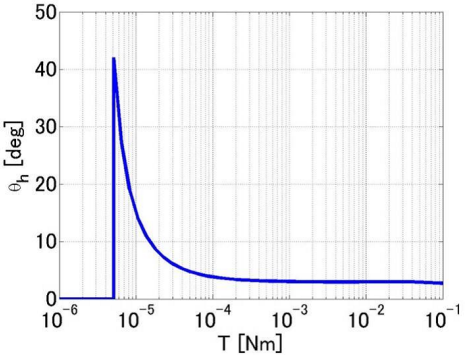

Figure 12. Hop Angle for Torque's Variation

velocity and achieve hopping mobility.

The force acted from the ground for time history is shown in Figure 10. The horizontal force has positive and negative values. When the body B leans at an angle more than a particular value, the rover obtains the opposite horizontal force from the ground. This is because the inertial force by deploying a rigid body A is larger than the pressing force by the torque.

Next, the behavior of the deployment rover is investigated when the input torque by DC motor is varied. Adding torque is a constant and given by T=10^{-6}∼10^{-1} [Nm]. The hop velocity and hop angle for applied torque's variation are shown in Figure 11 and Figure 12 respectively. Hopping angle is defined by the angle against the vertical direction. Figure 11 shows the applied torque has maximum and minimum because there are the gravity and the escape velocity. Hop angle is found almost unchanged for torque more than 10^{-4}[Nm] as shown in Figure 12. So, the rover can control not the hop angle but the hop speed by changing applied torque.

4.4 Optimal Deployment Rover Shape

The aspect ratio and the rate of the deployment part are investigated in the deployment rover shape.

The hop velocity and hop distance for the aspect ratio are shown by Figure 13 and Figure 14 respectively. Small aspect ratio shows the rover's shape is plane. On the other hand, large aspect ratio shows the shape is vertically long. According to these graphs, a plane shape rover has larger hop speed and hop distance than a vertically long shape rover. Additionally, the plane shape rover can obtain larger heat release area.

Figure 15 and Figure 16 show the hop velocity and hop distance for the rate of the deployment part respectively. The rate of deployment part $ratio_h$ is changed from 0.1 to 0.9. These graphs shows the rover with the large rate of the deployment part has larger hop velocity and hop distance. So, deploying the body side is more preferable. However, which side the rover deploys depends on the attitude of rover in landing. It is difficult that the rover control the attitude in landing under microgravity. Therefore, the rover can not choose which side the rover deploys. So, the rover which has the same deployment ratio is desirable.

5 Microgravity Experiment

In this section, the effectiveness of the deployment rover in terms of hop mobility is investigated by microgravity experiment. The comparison between experiment results and simulation results is performed. The microgravity experiments were conducted in the drop tower

”COSMOTORRE”[12] in Hokkaido, Japan. This drop tower has about 10^{-3}[G] for approximately 2.5[s].

5.1 Experimental Conditions

The prototype model of the deployment rover is shown in Figure 17. The prototype rover is constructed by the deployment part(Body A) and the body side(Body B). The deployment part is deployed by DC motor. The DC motor is controlled by MBED microcomputer. The specifications of the rover are shown by Table 3.

The DC motor is driven by PWM and controls the deployment's angle. A large angle command gives high torque. In this experiment, the deployment side is also changed in the body part and the deployment part. Body A or Body B is deployed by reversing the rover's side on the ground. The experiment conditions are shown by Table 4.

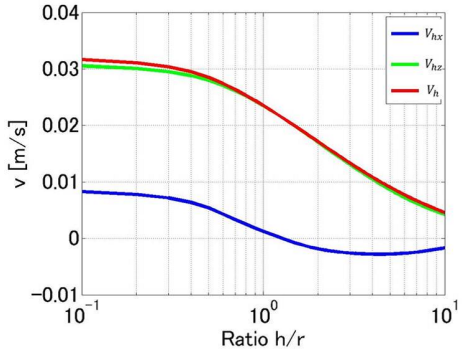

Figure 13. Hop Velocity for Aspect Ratio's Variation

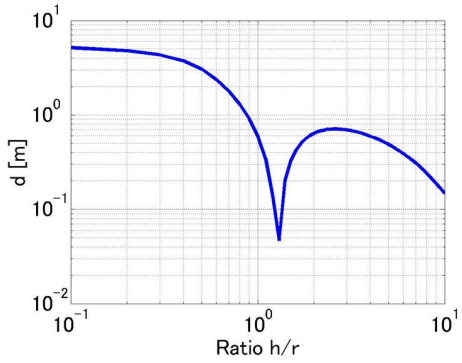

Figure 14. Hop Distance for Aspect Ratio's Variation

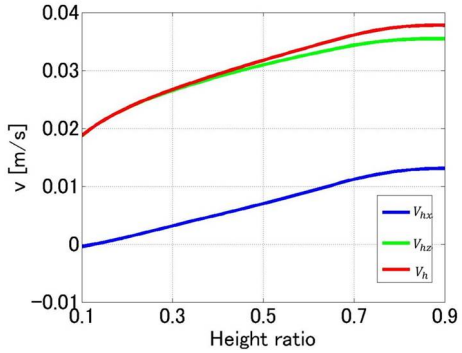

Figure 15. Hop Velocity for $ratio_h$'s Variation

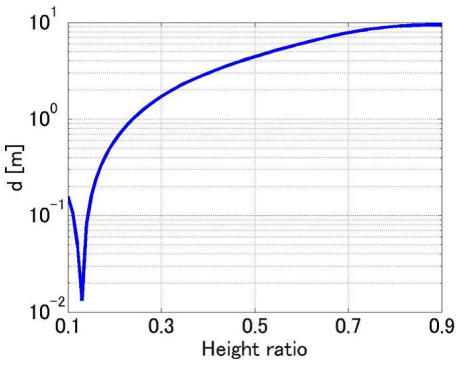

Figure 16. Hop Distance for $ratio_h$'s Variation

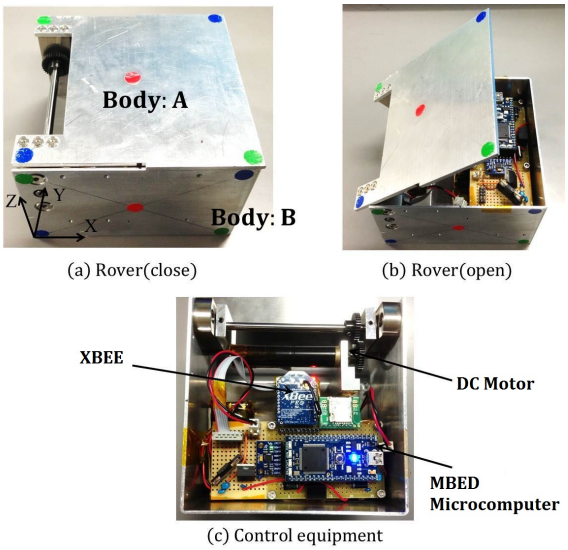

(a) Rover(close) (b) Rover(open)

(c) Control equipment

Figure 17. Prototype of Deployment Rover

Table 3. Specifications for Prototype Rover

Rover Size [mm]	Body A : 3(H)×120(W)×120(D) Body B : 70(H)×120(W)×120(D)
Rover Mass [g]	Body A : 140 Body B : 660
Rover Inertia [kgm^2]	Body A : 2.1×10^{-4} Body B : 9.6×10^{-4}
DC motor specification	Stall torque : 4.86[mNm] No load speed : 6300[rpm] Torque constant : 4.46[mNm/A] Gear ratio : 275:1

Table 4. Experimental Rover Conditions

Experiment	Deployment part	Angle Control
1	Body A	θ_{AB} = 20[deg]
2	Body B	θ_{AB} = 20[deg]
3	Body B	θ_{AB} = 60[deg]

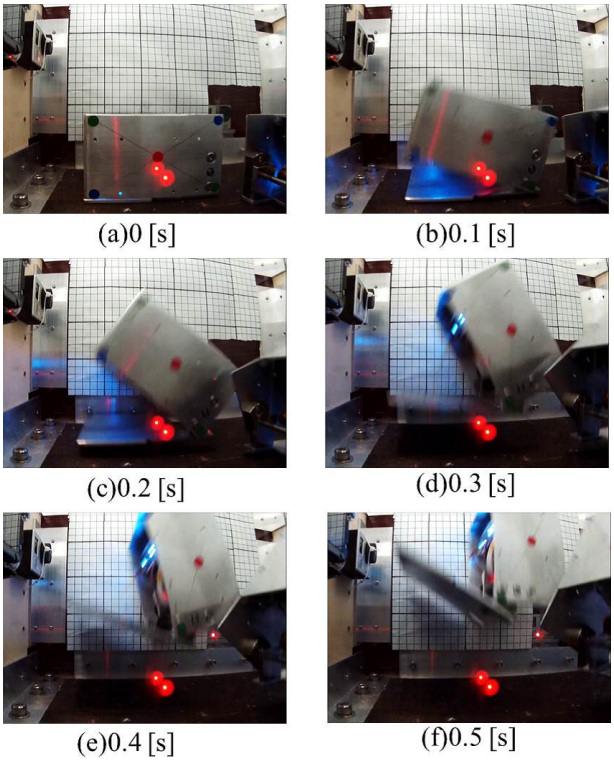

Figure 18. Overview of Hopping Motion (Experiment # 3)

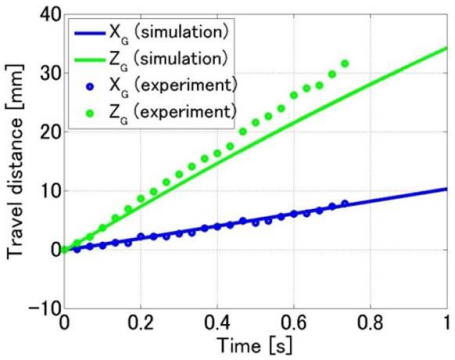

Figure 19. Travel Distance of Rover in Experiment 1

5.2 Experimental Results

An example motion of the deployment rover under microgravity is shown in Figure 18. The experiment condition of this example motion is "experiment # 3". These snapshots show the deployment rover can obtain horizontal and vertical velocity and achieve hopping mobility. So, this experiment shows the proposed deployment rover has a effective mobility on asteroid surface.

The comparisons between the experiment results and simulation results are shown in Figure 19, Figure 20, Figure 21. These graphs show the travel distance for time history in each experiment and simulation result. In this simulation, the rover model is adjusted to match the prototype rover. These results mean that the rover's motions in microgravity experiment is generally consistent with that in simulation though the simulation values tend to be larger than the experimental values. So, the validity of the model is indicated by these comparison. These errors are observed because the rover gets off the ground a little bit by initial vibration in drop.

The hop velocity and hop angle in microgravity ex-

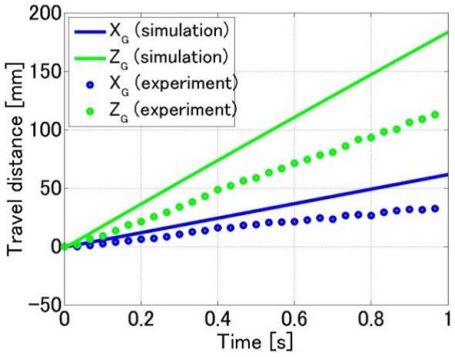

Figure 20. Travel Distance of Rover in Experiment 2

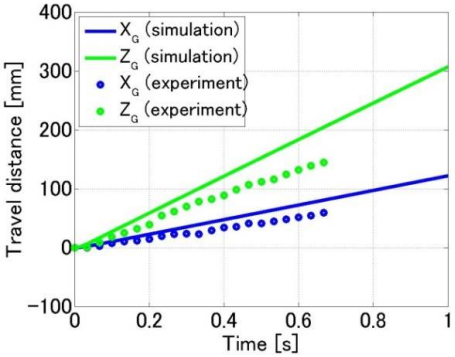

Figure 21. Travel Distance of Rover in Experiment 3

Table 5. Results of Microgravity Experiment

Experiment	θ_h[deg]	v_{hx}[mm/s]	v_{hz}[mm/s]
1	11.6	9.06	44.3
2	17.6	41.6	131
3	20.6	97.8	260

periment are shown in Table 5. The results of ”Experiment 1” and ”Experiment 2” show the rover can obtain the larger hop velocity and hop angle when the body side is deployed. In the results of ”Experiment 2” and ”Experiment 3”, the hop velocity changes accordingly when an applied torque is changed. This means the rover can control the hop velocity by controlling the deployment angle. Thus, the tendency of the experimental results is consistent with that of the simulation results discussed in sessions, 4.3 and 4.4.

6 Conclusions

In this paper, a new type of rover was proposed to move under microgravity as well as control its temperature by deploying the body of the rover. The effectiveness of the thermal control in the deployment model was investigated by using thermal mathematical model. The effectiveness of hop mobility under microgravity and the optimal design of the deployment rover were also investigated by 2D dynamics simulation respectively. Additionally, the effectiveness of the proposed rover in terms of hop mobility was also investigated by microgravity experiments. The validity of the model was shown by the comparison of experiment and simulation. So, these simulation and microgravity experiments show the deployment rover can hop under microgravity and control its temperature by deploying the body of the rover.

Acknowledgements

This work was supported by KAKENHI, Grant-in-Aid for Scientific Research(B) 24360101.

References

[1] T. Kubota, ”The first challenge in the world, Hayabusa project”, *Transactions of the Japan Society of Mechanical Engineers*, Vol.114, No.1107, 2011.

[2] T. Kubota, B. Wilcox , H. Saito, J. Kawaguchi, R. Jones, A. Fujiwara, J. Reverke, ”A Collaborative Micro-Rover Exploration Plan on the Asteroid Nereus in MUSEC-C Mission”, *In: 48th International Astronautical Congress*, 1997.

[3] T. Yoshimitsu, T. Kubota and I. Nakatani, ”New Mobility System of Exploration Rover for Small Planetary Bodies”, *Journal of the Robotics Society of Japan*, Vol.18, no.2, pp.292-299, 2000.

[4] K. Yoshida, ”The umping Tortoise: A Robot Design for Locomotion on Micro Gravity Surface”, *Proc. of 5th International Symposium on Artificial Intelligence. Robotics, Automation in Space*, pp.705-707, 1999.

[5] Y. Nakamura, S. Shimoda and S. Shoji, ”Mobility of a Microgravity Rover using Internal Electro-Magnetic Levitation”, *Proceedings of the 2000 IEEE/RSJ International Conference on Intelligent Robots and Systems*, 2000.

[6] S. Shimoda, T. Kubota and I. Nakatani, ”Proposal of New Mobility and Landing Experiment in Microgravity Experiment”, *Journal of the Japan Society for Aeronautical and Space Sciences*, Vol.53, No.614, pp.108-115, 2005.

[7] T. Yoshimitsu, T. Kubota and A. Adachi, ”MINERVA-Ⅱ surface exploration system in Hayabusa-2 asteroid explorer”, *The Japan society for Aeronautical and Space Sciences*, 4509, 2013.

[8] K.Yoshida, T.Maruki and H.Yano, ”A Novel Strategy for Asteroid Exploration with a Surface Robot”, *In proc. of the 3rd International conference on Field and service Robotics*, Finland, 281-286, June, 2002.

[9] M.Chacin, K.Yoshida, ”MULTI-LIMBED ROVER FOR ASTEROID SURFACE EXPLORATION USING STATIC LOCOMOTION”, *In Proc. of International symposium on Artificial Intelligence. Robotics, Automation in Space(i-SAIRAS05)*, ESA, Munich, Germany, pages. 1-8, 2005.

[10] T. Yoshimitsu, ”Planetary Rovers for Small Bodies”, *Journal of the Robotics Society of Japan*, Vol.21, No.5, pp.498-502, 2003.

[11] Yosuke Miyata, Tetsuo Yoshimitsu and Takashi Kubota, ”Progress of Research on A New Asteroid Exploration Rover Considering Thermal Control”, *The 2nd International Conference on Robot Intelligence Technology and Applications*, F1A, 2013.

[12] http://www.hastic.jp/